Remarkable Solvatochromic Color Change via Proton Tautomerism of a Phenol-Linked Imidazole Derivative

ARTICLE *in* THE JOURNAL OF PHYSICAL CHEMISTRY A · FEBRUARY 2014

Impact Factor: 2.69 · DOI: 10.1021/jp5007928 · Source: PubMed

2 AUTHORS, INCLUDING:

Jiro Abe
Aoyama Gakuin University
161 PUBLICATIONS **2,040** CITATIONS

SEE PROFILE

THE JOURNAL OF PHYSICAL CHEMISTRY A

Article

pubs.acs.org/JPCA

Remarkable Solvatochromic Color Change via Proton Tautomerism of a Phenol-Linked Imidazole Derivative

Hiroaki Yamashita and Jiro Abe*

Department of Chemistry, School of Science and Engineering, Aoyama Gakuin University, 5-10-1 Fuchinobe, Chuo-ku, Sagamihara, Kanagawa 252-5258, Japan

Supporting Information

ABSTRACT: A unique solvatochromic 2-phenyl-4,5-diarylimidazole derivative linked with a phenol moiety and a *p*-quinonemethide moiety at the 4- and 5-positions of a imidazole ring, which shows remarkable color change via proton tautomerism, was synthesized and the mechanism of the solvatochromic color change was investigated. The yellow-colored OH tautomeric form (**1_OH**) exists as a dominant species in nonpolar solvents, whereas the blue-colored NH tautomeric form (**1_NH**) is stabilized in polar solvents. The molecular structures of these tautomers were determined by X-ray crystallographic analysis. The *p*-quinonemethide moiety and the imidazole ring of **1_OH** are coplanar to one another and possess a planar quinoidal structure. On the other hand, **1_NH** has a nonplanar twisted quinoidal structure causing large bathochromic shift in the visible absorption spectrum. Moreover, the X-ray crystallographic analysis and the DFT calculations support the closed-shell singlet character of **1_OH**. In contrast **1_NH** possesses partial single bond character that leads to the open-shell singlet biradical character and the decrease in the singlet−triplet energy gap. The twisting of the π-conjugated electron system induced by the proton tautomerization was found to be the origin of the open-shell biradical character of **1_NH** and the enhanced solvatochromic color change.

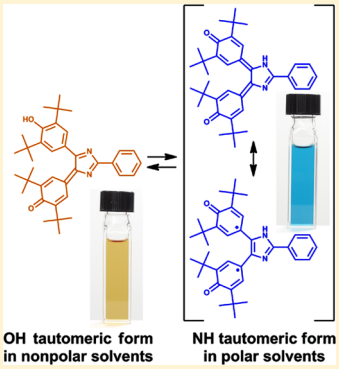

INTRODUCTION

Proton tautomerism has been of sustained interest because of its importance for understanding various chemical and biochemical phenomena ever since Lapworth's classic paper on acetone enolization over a century ago.[1−5] In the field of organic synthesis and biochemistry, many reaction mechanisms are explained by the proton tautomerism such as a keto−enol tautomerism.[6,7] From physicochemical point of view, proton tautomerism can be described by an intramolecular proton transfer reaction associated with a π-bond shifting. Besides, the position of an equilibrium is generally sensitive to the local environment of molecules. This implies that proton tautomerism has potential for switching the molecular properties of π-electron compounds by external stimuli such as light, heat, and solvent polarity.[8−15] It is noteworthy that π-bond shifting can drastically change the π-electronic structure and the corresponding physical properties such as dipole moment and molecular polarizability of a molecule. However, there are only a few examples of remarkable solvatochromic color change in the visible light region resulting from switching of the π-electronic structure by proton tautomerism. Furuta et al. reported the solvatochromism via proton tautomerism between the two types of tautomers for a N-confused porphyrin (NCP).[13] The significant solvatochromic color change of the NCP was explained on the basis of the pronounced alteration in the π-electronic structure by the proton tautomerization between the aromatic tautomer and the less-aromatic tautomer. 4-Nitoroso-5-aminopyrazole derivatives are also known to show the remarkable solvatochromic color change in the visible light region between the oxime red tautomer and the nitroso blue-green tautomer via proton tautomerism.[14]

Here we report a solvatochromic 2-phenyl-4,5-diarylimidazole derivative linked with a phenol moiety and a *p*-quinonemethide moiety at the 4- and 5-positions of a imidazole ring, that shows remarkable color change via proton tautomerism. In nonpolar solvents, the OH tautomeric form, **1_OH**, exists as a dominant species and shows yellow color. However, the blue-colored NH tautomeric form, **1_NH**, is stabilized with remarkable color change in polar solvents (Chart 1). We investigated the structure−property relationship of the solvatochromic imidazole to reveal the mechanism of the remarkable solvatochromic color change and found that **1_NH** has some open-shell character caused by the bond twisting despite purely closed-shell character of **1_OH**. We report that **1_NH** possess some open-shell singlet biradical character due to the twisting of the π-conjugated electron system induced by proton tautomerization and propose a new concept for switching π-electronic structures by solvent polarity.

EXPERIMENTAL SECTION

Synthesis. All reactions were monitored by thin-layer chromatography carried out on 0.2 mm E. Merck silica gel

Received: January 23, 2014
Revised: February 7, 2014
Published: February 10, 2014

   dx.doi.org/10.1021/jp5007928 | *J. Phys. Chem. A* 2014, 118, 1430−1438

Chart 1

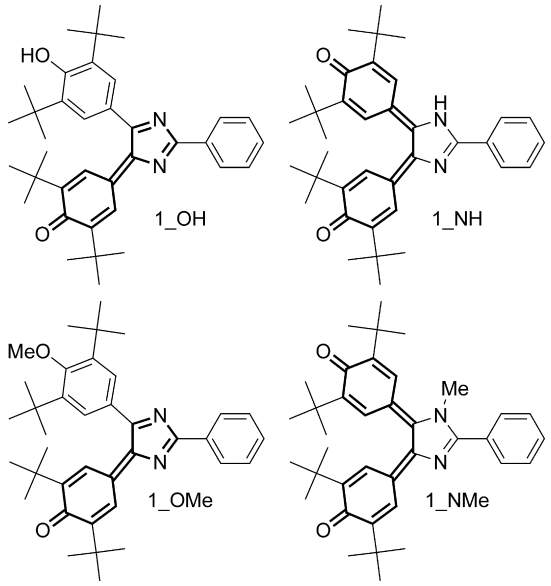

plates (60F-254). Column chromatography was performed on silica gel (Wakogel C-300). ^{1}H NMR spectra were recorded at 400 MHz on a Bruker AVANCE III 400 NanoBay. Acetone-d_6, DMSO-d_6, and $CDCl_3$ were used as deuterated solvent. ESI−TOF−MS spectra were recorded on a Bruker micrOTOF II-AGA1. All glassware was washed with distilled water and dried. Unless otherwise noted, all reagents and reaction solvents were purchased from TCI, Wako Co. Ltd., Aldrich Chemical Co., Inc., and ACROS Organics and were used without further purification.

1,2-Bis(3,5-di-*tert*-butyl-4-hydroxyphenyl)ethane-1,2-dione (2). To a solution of 2,6-di-*tert*-butylphenol (1.0 g, 5.61 mmol) in dry dichloromethane (30 mL) under nitrogen stirred at 0 °C was added oxalylchloride (0.29 mL, 3.38 mmol) and the reaction mixture was stirred at 0 °C for 10 min. Then, $AlCl_3$ (898 mg, 6.73 mmol) was added and the reaction mixture was stirred at 0 °C for 30 min. The reaction mixture was allowed to warm to room temperature and was stirred at room temperature overnight. The reaction mixture was poured into water and the organic layer was extracted with dichloromethane. The organic layer was dried over Na_2SO_4, filtered, and then concentrated in vacuo. The crude product was purified by recrystallization (dichloromethane/hexane) to give a yellow crystal (**2**), 481 mg (1.03 mmol, 37%). ^{1}H NMR (400 MHz, $CDCl_3$, δ): 7.85 (s, 4H), 5.89 (s, 2H), 1.45 (s, 36H). ESI−TOF−MS (m/z): 489 $[M + Na]^+$.

4,4′-(2-Phenyl-1*H*-imidazole-4,5-diyl)bis(2,6-di-*tert*-butylphenol) (1_L). Compound **2** (170.6 mg, 0.366 mmol), benzaldehyde (38.6 mg, 0.364 mmol), and ammonium acetate (130.0 mg, 1.69 mmol) were refluxed in acetic acid (5 mL) for 28 h. The reaction mixture was cooled to room temperature and the slurry that precipitated by the neutralization the mixture by aqueous NH_3 was filtered off. The residue was purified by silica gel column chromatography $CHCl_3$ as eluent to give a white powder (**1_L**), 168 mg (0.328 mmol, 90%). ^{1}H NMR (400 MHz, DMSO-d_6, δ): 12.73 (s, 1H), 8.00 (d, J = 7.5 Hz, 2H), 7.44 (t, J = 7.3 Hz, 4H), 7.32 (s, 3H), 7.15 (s, 2H), 7.09 (s, 1H), 6.70 (s, 1H), 1.35 (s, 18H), 1.28 (s, 18H). ESI−TOF−MS (m/z): 553 $[M + H]^+$.

2,6-Di-*tert*-butyl-4-[5-(3,5-di-*tert*-butyl-4-hydroxyphenyl)-2-phenyl-4*H*-imidazole-4-ylidene]cyclohexa-2,5-dienone (1_OH). To a solution of **1_L** (39.0 mg, 0.071 mmol) in benzene (4 mL) under nitrogen stirred at room temperature was added PbO_2 (44.0 mg, 0.18 mmol) and the reaction mixture was stirred at room temperature for 2.5 h. PbO_2 was filtered off and the filtrate was concentrated in vacuo. The crude product was purified by silica gel column chromatography benzene as eluent to give a dark red solid (**1_OH**), 28.1 mg (0.0510 mmol, 71%). ^{1}H NMR (400 MHz, $CDCl_3$, δ): 8.56 (d, J = 8.0 Hz, 2H), 7.58−7.50 (m, 3H), 7.42 (s, 2H), 7.36 (s, 1H), 7.32 (d, J = 2.3 Hz, 1H), 5.57 (s, 1H), 1.47 (s, 18H), 1.41 (s, 9H), 1.04 (s, 9H). ESI−TOF−MS (m/z): 551 $[M + H]^+$.

1-(3,5-Di-*tert*-butyl-4-hydroxyphenyl)-2-(3,5-di-*tert*-butyl-4-methoxyphenyl)ethane-1,2-dione (2_OMe). To a suspension of **2** (50.0 mg, 0.107 mmol) and potassium carbonate (15 mg, 0.108 mmol) in dry acetone (10 mL) was added methyl iodide (10 μL, 0.161 mmol). After being refluxed for 4 h, the reaction mixture was cooled to room temperature and concentrated in vacuo. The reaction mixture was dissolved in CH_2Cl_2 and washed with water. The organic layer was dried over Na_2SO_4, filtered, and then concentrated in vacuo. The crude product was purified by silica gel column chromatography hexane/CH_2Cl_2 = 1:1 as eluent to give a white powder (**2_OMe**), 20.4 mg (0.0428 mmol, 40%). ^{1}H NMR (400 MHz, $CDCl_3$, δ): 7.89 (s, 2H), 7.85 (s, 2H), 5.90 (s, 1H), 3.74 (s, 3H), 1.45 (s, 18H), 1.42 (s, 18H). ESI−TOF−MS (m/z): 503 $[M + Na]^+$.

2,6-Di-*tert*-butyl-4-(5-(3,5-di-*tert*-butyl-4-methoxyphenyl)-2-phenyl-1*H*-imidazol-4-yl)phenol (1_L_OMe). The compound **2_OMe** (20.0 mg, 0.0416 mmol), benzaldehyde (25.0 mg, 0.236 mmol), and ammonium acetate (44.0 mg, 0.571 mmol) were refluxed in acetic acid (3 mL) for 24 h. The reaction mixture was cooled to room temperature and the slurry that precipitated by the neutralization the mixture by aqueous NH_3 was filtered off. The residue was washed with hexane to give a white powder (**1_L_OMe**), 10.0 mg (0.328 mmol, 42%). ^{1}H NMR (400 MHz, DMSO-d_6) mixture of two diastereomers δ: 12.48 (s, 1H, one diastereomer), 12.2 (s, 1H, one diastereomer), 7.63 (s, 1H, one diastereomer), 7.48−7.42 (m, 4H, one diastereomer), 7.35 (s, 4H, one diastereomer), 7.28 (s, 2H, one diastereomer), 7.22 (s, 2H, one diastereomer), 7.16 (s, 2H, one diastereomer), 7.10 (s, 2H, one diastereomer), 1.36−1.28 (m, 72H, two diastereomers). ESI−TOF−MS (m/z): 565 $[M - H]^-$.

2,6-Di-*tert*-butyl-4-[5-(3,5-di-*tert*-butyl-4-methoxyphenyl)-2-phenyl-4*H*-imidazol-4-ylidene]cyclohexa-2,5-dienone (1_OMe). To a solution of **1_L_OMe** (23.1 mg, 0.0408 mmol) in benzene (3 mL) under nitrogen stirred at room temperature was added PbO_2 (98.6 mg, 0.412 mmol) and the reaction mixture was stirred at room temperature for 6 h. PbO_2 was filtered off and the filtrate was concentrated in vacuo. The crude product was purified by silica gel column chromatography benzene as eluent to give a dark red solid (**1_OMe**), 11.0 mg (0.0192 mmol, 47%). ^{1}H NMR (400 MHz, $CDCl_3$, δ): 8.56 (d, J = 6.6 Hz, 2H), 8.44 (d, J = 1.2 Hz, 1H), 7.53−7.51 (m, 3H), 7.46 (s, 1H), 7.36 (s, 3H), 1.46 (s, 18H), 1.40 (s, 9H), 1.03 (s, 9H). ESI−TOF−MS (m/z): 565 $[M + H]^+$.

4,4′-(1-Methyl-2-phenyl-1*H*-imidazole-4,5-diylidene)-bis(2,6-di-*tert*-butylcyclohexa-2,5-dienone) (1_NMe). To a suspension of **1_NH** (50.0 mg, 0.107 mmol) and potassium

dx.doi.org/10.1021/jp5007928 | J. Phys. Chem. A 2014, 118, 1430−1438

Scheme 1

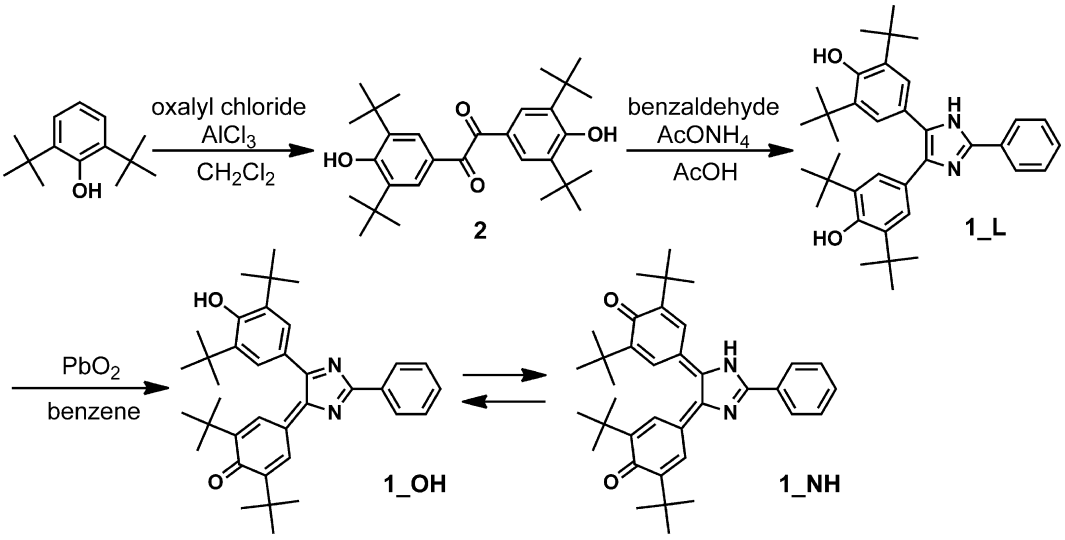

carbonate (15 mg, 0.108 mmol) in dry acetone (10 mL) was added dimethyl sulfate (10 μL, 0.161 mmol). After being refluxed for 2 h, the reaction mixture was cooled to room temperature and concentrated in vacuo. The reaction mixture was dissolved in CH_2Cl_2 and washed with water. The organic layer was dried over Na_2SO_4, filtered, and then concentrated in vacuo. The crude product was purified by silica gel column chromatography benzene as eluent to give a dark blue solid (**1_NMe**), 20.4 mg (0.0428 mmol, 40%). ^{1}H NMR (400 MHz, DMSO-d_6, δ): 8.20 (s, 1H), 7.91 (d, J = 7.5 Hz, 2H), 7.68−7.63 (m, 3H), 7.29 (s, 2H), 6.95 (s, 1H), 1.33 (s, 9H), 1.21 (s, 18H), 1.13 (s, 9H). ESI−TOF−MS (m/z): 565 $[M + H]^+$.

X-ray Crystallographic Analysis. The diffraction data of the single crystal was collected on the Bruker APEX II CCD area detector (Mo Kα, λ = 0.71073 nm). The data refinement was carried out by the Bruker APEXII software package with SHELXT program.[16,17] All non-hydrogen atoms were anisotropically refined.

DFT Calculation. All calculations were carried out using the Gaussian 09 program (Revision D.01).[18] The molecular structures were fully optimized at the (U)B3LYP/6-31+G(d,p) and the PCM−DFT B3LYP/6-31+G(d,p) levels of the theory, and analytical second derivatives were computed using vibrational analysis to confirm each stationary point to be a minimum. The TDDFT calculations were performed at the B3LYP/6-31+G(d,p) level of the theory for the optimized geometries obtained by the (U)B3LYP/6-31+G(d,p) method.

RESULTS AND DISCUSSION

Solvatochromism and Molecular Structures of Tautomers. The oxidation of the imidazole precursor **1_L** with PbO_2 in benzene gives dark yellow solution of **1_OH** (Scheme 1). However, **1_OH** gives dark blue solutions when dissolved in polar solvents such as methanol, acetone, and dimethylsulfoxide (DMSO) despite giving dark yellow color in nonpolar solvents such as hexane, benzene, and dichloromethane (Supporting Information Figure S2). As shown in Figure 1a, the dichloromethane and acetone solutions of **1_OH** show typical solution colors in nonpolar and polar solvent, respectively. The remarkable color change of the solutions suggests a presence of a proton tautomeric equilibrium between **1_OH** and another tautomer **1_NH**, which is shown in Chart 1. The UV−vis absorption spectra of **1_OH** dissolved in a series of dichloromethane/acetone binary mixture with different volume ratio were measured to investigate the influence of the solvent polarity. The pure dichloromethane solution shows the absorption peak at 433 nm as shown in Figure 1b. With increasing the solvent polarity, the absorption band around at 433 nm decreases, while the absorption band around at 656 nm increases. These spectral changes are continuous and imply the presence of the equilibrium between two species. To identify each species in polar and nonpolar solvents, the ^{1}H and ^{13}C NMR spectra were examined (Supporting Information Figures S4−S7). In $CDCl_3$ at room temperature, there is a characteristic ^{1}H NMR signal at 5.6 ppm assignable to the phenolic OH, indicating **1_OH** is the dominant species in nonpolar solvent. A downfield ^{13}C NMR signal at 187.0 ppm is attributable to the

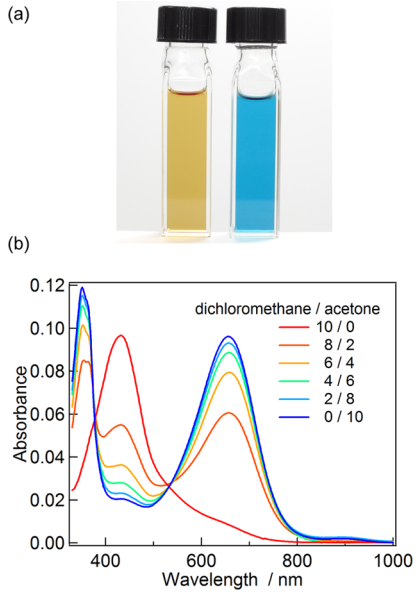

Figure 1. (a) The dichloromethane solution (left) and acetone solution (right) in the tautomeric equilibrium between **1_OH** and **1_NH**. (b) UV−vis absorption spectra for the solutions in the tautomeric equilibrium in the binary mixture of dichloromethane/acetone. The volume ratios of two solvents are shown in legends. All spectra were measured at the same concentration (2.4×10^{-4} M).

dx.doi.org/10.1021/jp5007928 | J. Phys. Chem. A 2014, 118, 1430−1438

Scheme 2

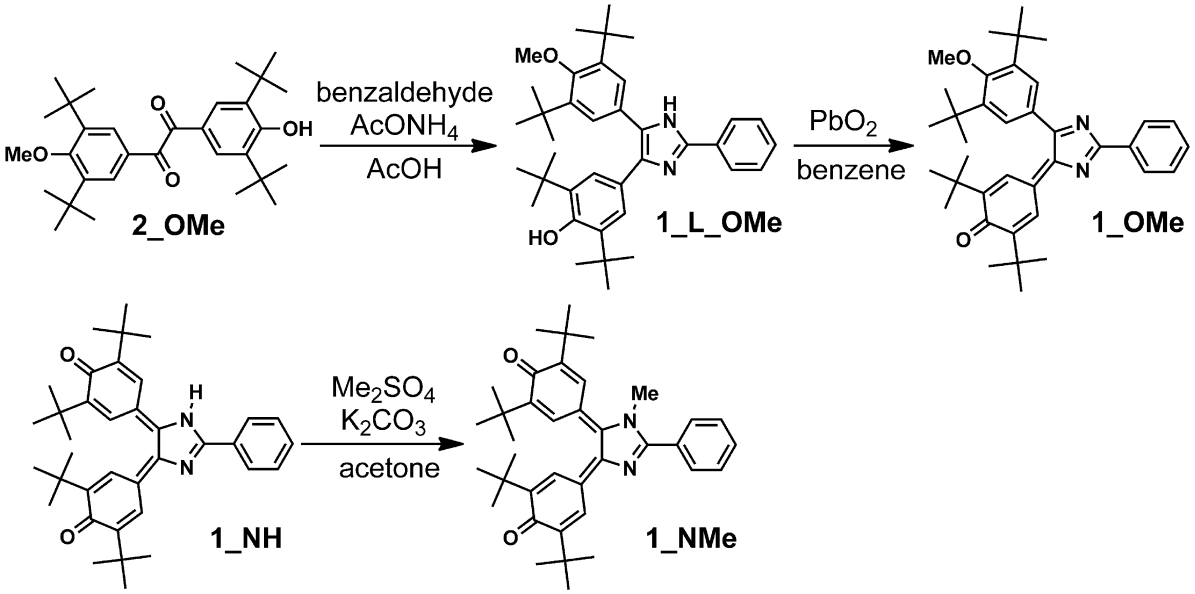

carbonyl carbon of the *p*-quinonemethide moiety, which is consistent with the structure of **1_OH**. The ^{13}C NMR signals at 178.3 and 173.0 ppm can be assigned to the two carbons of the C═N double bonds, which also support that **1_OH** is dominant species in nonpolar solvents. On the other hand, the ^{1}H and ^{13}C NMR spectra in acetone-d_6 are completely different from those in $CDCl_3$. The broadening of the ^{1}H NMR signals are observed for all protons except for the protons in phenyl rings at room temperature (Supporting Information Figure S5a). In addition, only the ^{13}C NMR signals attributable to the carbons in the phenyl rings and *tert*-butyl groups were observed at room temperature (Supporting Information Figure S5b). The reason for these spectral behaviors will be discussed later in detail. In order to prevent the signal broadening, the ^{1}H and ^{13}C NMR spectra in acetone-d_6 were measured at low temperature. The ^{1}H NMR signals became sharp with decreasing the temperature, and a characteristic downfield signal at 12.3 ppm assignable to the imidazole NH is observed at −60 °C (Supporting Information Figure S5a). The two downfield ^{13}C NMR signals were observed at 186.6 and 185.5 ppm (Supporting Information Figure S5b). These signals indicate the presence of two carbonyl carbons of the *p*-quinonemethide moieties, which is consistent with the structure of **1_NH**. Therefore, we concluded that the dominant species in polar solvents is **1_NH**.

By comparing the UV−vis absorption spectrum of **1_OH** in basic methanol (Supporting Information Figure S7), the absorption band around at 900 nm observed in acetone can be assigned to an anionic intermediate (Supporting Information Scheme S1). This band can be observed even though dry acetone is used as a solvent, indicating that acetone is protonated by **1_OH** (Supporting Information Figure S3). The origin of strong acidity of **1_OH** is considered to be the thermal stabilization of the anionic species by charge delocalization.

To obtain clear evidence for the presence of the proton tautomeric reaction, *O*- and *N*-methylated derivatives (**1_OMe** and **1_NMe**), which are inactive against the proton tautomeric reaction in both polar and nonpolar solvents, were synthesized (Scheme 2). The UV−vis absorption spectra of **1_OMe** and **1_NMe** in hexane and acetone are shown in Figure 2a. The absorption spectra of **1_OMe** and **1_NMe**, respectively, are

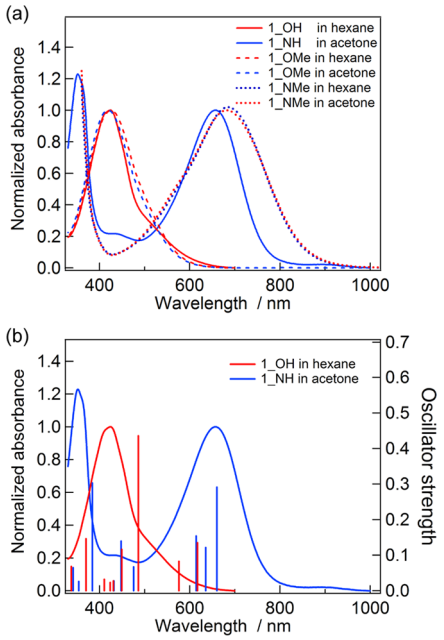

Figure 2. (a) UV−vis absorption spectra for **1_OMe** (dichloromethane solution, red dashed line; acetone solution, blue dashed line), and **1_NMe** (dichloromethane solution, red dotted line; acetone solution, blue dotted line). Solid lines are UV−vis absorption spectra for the solution in the tautomeric equilibrium between **1_OH** and **1_NH** in dichloromethane (red solid line) and acetone (blue solid line). (b) Experimental and theoretical UV−vis absorption spectra for **1_OH** and **1_NH**. The calculated spectra (B3LYP/6-31+G(d,p)) are shown by the perpendicular lines.

similar to those of **1_OH** and **1_NH**, giving clear evidence that the spectral changes by changing the solvent polarity are caused by the proton tautomeric equilibrium between two tautomers.

We investigated the driving force of the proton tautomeric reaction by using the DFT calculations including the bulk

dx.doi.org/10.1021/jp5007928 | J. Phys. Chem. A 2014, 118, 1430−1438

solvent effect by the polarized continuum model (DFT−PCM). The molecular structures were fully optimized in heptane (ε = 1.92), acetone (ε = 20.7), and DMSO (ε = 46.7) at the PCM/B3LYP/6-31+G(d,p) level of the theory. The changes in Gibbs free energies ΔG° of the tautomeric reaction from **1_OH** to **1_NH** are +7.92, +6.25, −1.24, and −2.38 kJ/mol in gas phase, heptane, acetone, and DMSO, respectively (Supporting Information Figure S10). The ΔG° values show that **1_OH** is thermally more stable than **1_NH** in gas phase or nonpolar solvents. However, it is predicted that the relative thermal stabilities would reverse in polar solvents and **1_NH** becomes more stable than **1_OH**. This regular shift of the ΔG° values of the tautomers predicted by the DFT−PCM calculations is consistent with the experimental observations. The energetic preferences of **1_OH** in nonpolar solvent and **1_NH** in polar solvent can be explained as follows. In gas phase or nonpolar solvents, **1_OH** is more stable than **1_NH** because of the aromatic stabilization energy. However, in polar solvents, **1_NH** is largely stabilized by solvent−solute electrostatic interaction because the electric dipole moment of **1_NH** is larger than that of **1_OH**. The calculated dipole moments in gas phase (B3LYP/6-31+G(d,p)) of **1_NH** and **1_OH** are 8.22 and 4.89 D, respectively.

The theoretical absorption spectra of **1_OH** and **1_NH** calculated by the TDDFT (B3LYP/6-31+G(d,p)) method are shown in Figure 2b along with the experimental absorption spectra in hexane and acetone. The calculation results explain well the experimental observations and support the experimental result that **1_OH** and **1_NH** are the dominant species in nonpolar and polar solvents, respectively. The $S_0 \rightarrow S_3$ transition (f = 0.4357) at 486 nm of **1_OH** is attributable to the HOMO−1 → LUMO transition which is described by the transition from the phenol moiety with electron-donating characteristics to the *p*-quinonemethide moiety with electron-withdrawing characteristics (Figure 3). On the other hand, the $S_0 \rightarrow S_1$ transition (f = 0.2911) at 660 nm of **1_NH** is attributable to the HOMO → LUMO transition, described by the $\pi \rightarrow \pi^*$ transition of the two *p*-quinonemethide moieties linked by the imidazole ring. These calculation results support that the proton tautomeric reaction causes a large change in the π-electronic structure and results in the drastic color change. The tautomerization process from **1_OH** to **1_NH** loses the aromatic phenol moiety and forms the *p*-quinonemethide moiety. This tautomerization process leads to the breaking of the *p*-quinoid structure composed of the *p*-quinonemethide moiety and the imidazole ring in **1_OH** and the formation of a long π-conjugated moiety consisted of the two *p*-quinonemethide moieties, resulting in the large bathochromic shift in the visible absorption spectrum through the proton tautomerization.

Moreover, we found that the TDDFT calculation (B3LYP/6-31+G(d,p)) for a model compound, **1_NH_model** in which all *tert*-butyl groups are removed from **1_NH**, predicts that the $S_0 \rightarrow S_1$ transition (f = 0.4822) is located at 575 nm, which is much shorter than the $S_0 \rightarrow S_1$ transition (660 nm, f = 0.2911) of **1_NH** calculated by the same level of the theory (Supporting Information Figure S11). The interpretation of this hypsochromic shift of the absorption spectrum of **1_NH_model** is as follows. The calculated HOMO−LUMO energy gap of **1_NH_model** is larger than that of **1_NH**, implying that the steric hindrance caused by the bulky *tert*-butyl groups affects the energy levels of the frontier molecular orbitals. The HOMO and LUMO, respectively, exhibit bonding and antibonding

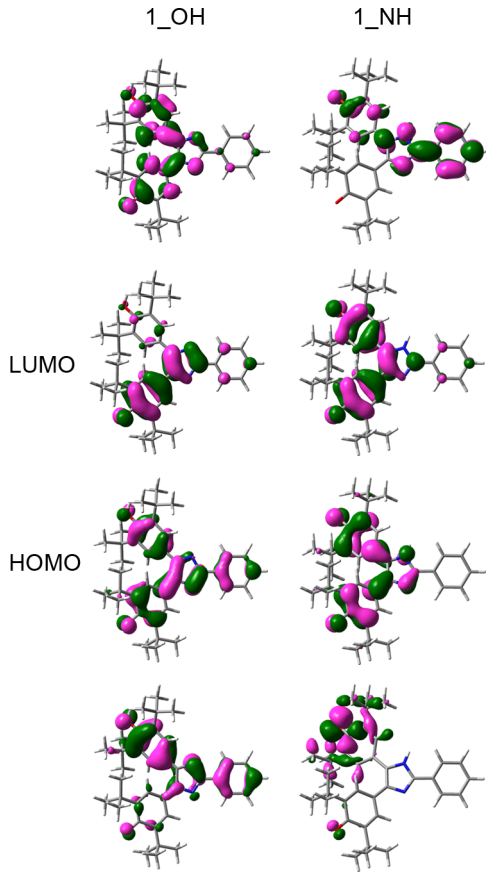

Figure 3. Relevant molecular orbitals of **1_OH** and **1_NH** obtained at the B3LYP/6-31+G(d,p) level of the theory.

characters with respect to the two C═C double bonds between the imidazole ring and the *p*-quinonemethide moieties. Thus, it is expected that the resonance integral decreases with increasing the twisting angles of the C═C double bonds. Thus twisting of the C═C double bonds leads to raising the HOMO energy and lowering the LUMO energy as illustrated in Figure 4.[19,20] For example, in a twisted ethylene model the double bond character decreases with increasing the twisting angle of the C═C double bond. In a 90° twisted ethylene, the HOMO−LUMO energy gap vanishes and consequently two degenerate orbitals localized on two carbon atoms are formed.[21] The ground electronic state of the 90° twisted ethylene is the triplet biradical state according to Hund's rule. Furthermore, the oscillator strength of the HOMO → LUMO transition would be getting close to zero with increasing the twisting angle of the C═C double bond because of decreasing the orbital overlap between the adjacent π orbitals. Actually, the oscillator strength of the $S_0 \rightarrow S_1$ transition of **1_NH** (f = 0.2911) is smaller than that of **1_NH_model** (f = 0.4822). The reason why the chromophore of **1_NH** shows the absorption band in near-infrared region despite the short π-conjugated length is the twisting of the π-conjugated chromophore. Thus the twisting of a π-conjugated moiety is found to be effective to shift the absorption maximum to the longer wavelength region though the absorption intensity will be sacrificed.

The molecular structures of the **1_OH** and **1_NH** were determined by single crystal X-ray crystallographic analysis (Figure 5). The deep red crystals of **1_OH** suitable for X-ray crystallographic analysis were prepared by recrystallization from benzene. The bond lengths and torsion angles are summarized

dx.doi.org/10.1021/jp5007928 | J. Phys. Chem. A 2014, 118, 1430−1438

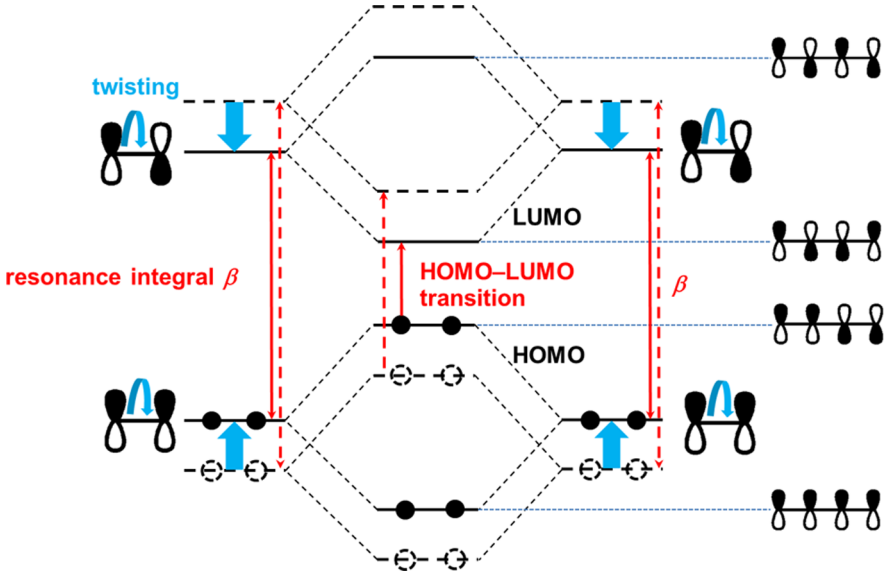

Figure 4. The effect of twisting the double bond on the energy levels of the frontier molecular orbitals of a butadiene unit.

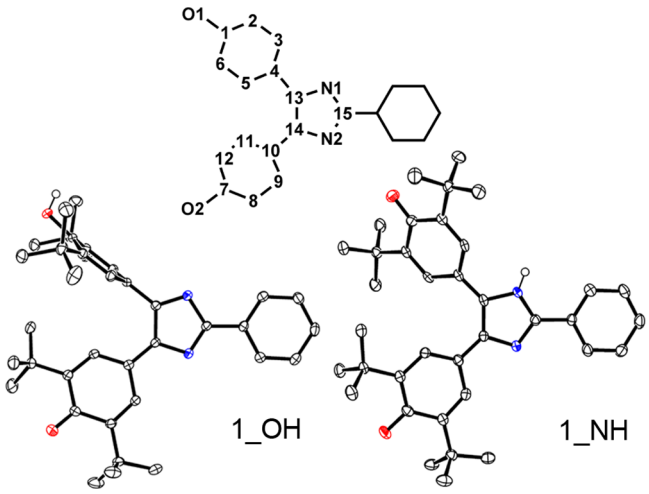

Figure 5. ORTEP representation of the molecular structures of **1_OH** and **1_NH** with thermal ellipsoids (50% probability) where nitrogen and oxygen atoms are highlighted in blue and red, respectively. The hydrogen atoms on the phenyl rings and *tert*-butyl groups, and the solvent molecules are omitted for clarity.

in Table 1. The C1−O1 bond length (1.381 Å) is consistent with a typical bond length for the C−O single bond. The C7−O2 (1.226 Å), C13−N1 (1.307 Å), and C15−N2 (1.308 Å) are also consistent with the bond lengths for the usual C═O and C═N double bonds, suggesting that **1_OH** has planar quinoidal structure as shown in Figure 5. The phenol ring is almost orthogonal to the imidazole ring (the dihedral angle N1−C13−C4−C3 = 91.9°) due to the formation of the cyclic hydrogen-bonded dimer with neighboring molecules in which two O−H−N hydrogen bonds between the phenol groups and the imidazole rings are formed. On the other hand, the deep blue crystals of **1_NH** were obtained by recrystallization from DMSO. The hydrogen bond between the imidazole NH and the oxygen atom of DMSO was observed (2.874 Å), suggesting that **1_NH** is stabilized through the hydrogen bonding formation in polar solvent compared with **1_OH**. The comparison of the bond lengths between **1_NH** and **1_OH** reveals a notable structural feature of **1_NH**. The C═O double bonds of **1_NH**, C1−O1 (1.246 Å) and C7−O2 (1.248 Å) are slightly longer than the C7−O2 bond of **1_OH** (1.226 Å). The bond lengths of the C4−C13 (1.404 Å) and C10−C14 (1.401 Å) are longer than the C10−C14 bond of **1_OH** (1.384 Å). Another notable feature is large torsion angle of the C4−C13 double bond (C5−C4−C13−C14 = 32.4°), which shows

Table 1. Selected Bond Lengths (Å) and Dihedral Angles (deg) for 1_OH and 1_NH Obtained by the X-ray Crystallographic Analysis and the DFT Calculations

	1_OH (X-ray)	**1_OH** (DFT)	**1_NH** (X-ray)	**1_NH** (DFT CS)	**1_NH** (DFT SBR)
N1−C13	1.307	1.313	1.385	1.390	1.388
C13−C14	1.478	1.495	1.455	1.460	1.446
C14−N2	1.386	1.380	1.393	1.389	1.385
N2−C15	1.308	1.320	1.314	1.310	1.314
C15−N1	1.426	1.405	1.373	1.385	1.381
C4−C13	1.485	1.468	1.404	1.403	1.416
C10−C14	1.384	1.395	1.401	1.408	1.422
O1−C1	1.381	1.371	1.246	1.243	1.246
O2−C7	1.226	1.237	1.248	1.241	1.244
C5−C4−C13−C14	82.7	43.2	32.4	21.44	24.0
C11−C10−C14−C13	9.9	9.6	0.1	15.18	18.2

dx.doi.org/10.1021/jp5007928 | *J. Phys. Chem. A* 2014, 118, 1430−1438

marked distortion due to the steric repulsion between bulky *tert*-butyl groups. These structural features indicate that the C═C and C═O double bonds in **1_NH** have partial single bond character, implying a certain contribution of open-shell singlet biradical (SBR) character. The SBR character generally increases with decreasing the overlap integral between the two adjacent π-orbitals.[22,23] For comparison, the theoretical bond lengths of the closed-shell (CS) and SBR states of **1_NH** were calculated at the (U)B3LYP/6-31+G(d,p) level of the theory. The calculated result for the CS state well explains the molecular geometry of **1_NH** experimentally determined by single crystal X-ray crystallographic analysis. Therefore, we considered that the ground state electronic structure of **1_NH** is the CS singlet or the singlet state with small contribution from the open-shell biradical resonance form. The energies of each electronic structure will be discussed in the next section.

Open-Shell Character of 1_NH. Judging from the bond lengths determined by the X-ray crystallographic analysis, **1_NH** has weak double bonds due to the distortion by the steric hindrance between the *tert*-butyl groups. The nature of twisted double bonds has been intensely studied from the standpoint of its nonlinear optical properties[24] and importance to understand the bond-breaking process of π-conjugated electron systems.[25] It is generally known that twisted double bonds possess a certain contribution of SBR state because of admixing of the doubly excited electronic configuration into the ground state and result in small singlet−triplet energy gap (ΔE_{S-T}) due to relatively small exchange integral.[22,23]

For the better understanding of the experimental results, we performed theoretical investigation of the electronic structure of **1_NH**. The DFT calculations were conducted at the (U)B3LYP/6-31+G(d,p) level of the theory for the CS, the SBR, and the triplet biradical (TBR) states of **1_NH**. The wave function of the SBR state were obtained by using the broken-symmetry DFT method.[26−28] The SBR state of **1_NH** was calculated to be the lowest energy state with the spin-squared expectation value $\langle S^2 \rangle$ = 0.3716 and the $\Delta E = E(\mathrm{CS}) - E(\mathrm{SBR})$ = 0.9 kcal mol^{-1} where E(CS) and E(SBR) are the zero-point corrected total energies of the CS and SBR states, respectively. The singlet−triplet energy gap ΔE_{S-T} of **1_NH** was estimated to be 5.7 kcal mol^{-1}. However, the optimized geometry of the CS state of **1_NH** well explains the geometry obtained by X-ray crystallographic analysis and the IR spectrum, which means the ground-state electronic structure of **1_NH** can be described by the CS state with small contribution from the SBR state. The total spin density distribution of the SBR and TBR states of **1_NH** are shown in Supporting Information Figure S8. The singlet biradical character (y) of the electronic ground singlet state of **1_NH** was calculated to be 22% from the LUMO occupation number of 0.22 by the CASSCF(8,8)/6-31G(d)//RB3LYP/6-31+G-(d,p) level of the theory. These results suggest that the ground electronic state of **1_NH** can be regarded as a singlet state with small contribution of the open-shell biradical character.

The FT−IR spectroscopy also provides helpful information on the ground state electronic structures of **1_OH** and **1_NH**. The IR absorption spectra in the fingerprint region of the crystalline **1_OH** and **1_NH** are shown in Figure 6. The intense absorption band at 1622 cm^{-1} in **1_OH** corresponds to the C═O stretching vibrational mode of the *p*-quinonemethide moiety. This indicates that the C═O double bond of **1_OH** is regarded as a pure double bond. On the other hand, the C═O stretching vibrational mode of **1_NH** is observed at 1558 cm^{-1}.

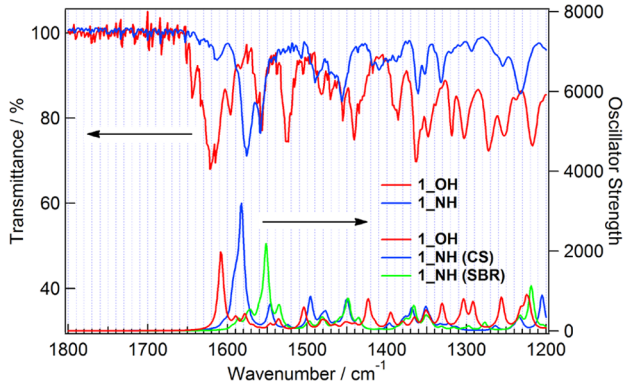

Figure 6. IR absorption spectra for the solid state **1_OH** and **1_NH** and the theoretical IR spectra for **1_OH** and **1_NH** at (U)B3LYP/6-31+G(d,p) level of the theory.

This value lies between the wavenumber for the typical phenoxyl radical (1481 cm^{-1})[29] and that for the C═O double bond of **1_OH** (1622 cm^{-1}), indicating that the twisting of the C═C double bonds weaken the double bond character of the C═O bonds of **1_NH**. As shown in Figure 6, the experimental IR spectra are in good agreement with the theoretical IR spectra obtained by the DFT calculations for **1_OH** and the CS state for **1_NH** at the B3LYP/6-31+G(d,p) level of the theory. Thus, the ground state electronic structure of **1_NH** can be considered as the CS state rather than the pure open-shell biradical state.

The ESR spectroscopy gives direct information for the thermally excited triplet state of **1_NH**. The ESR spectra were measured by using the quartz capillary tube containing a DMSO solution since **1_NH** is the dominant species in polar solvent. The DMSO solution of **1_NH** exhibits weak ESR signal at room temperature (Supporting Information Figure S9). The temperature dependence of the ESR spectra is shown in Figure 7. The ESR signal intensities I_{ESR}, which were

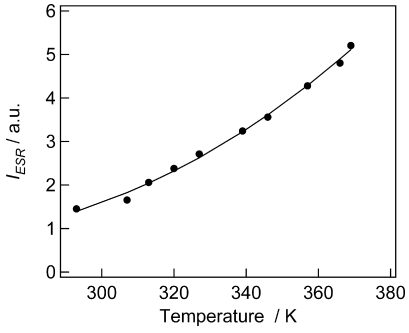

Figure 7. Temperature dependence of the ESR signal intensity of **1_NH** in DMSO. The solid line represents the fit to the Bleaney−Bowers equation for the two-site Hisenberg Hamiltonian.

obtained by using double integration of the first derivative spectra, increases with heating the solution from room temperature to 100 °C, indicating that the population of thermally excited triplet state increases with raising the temperature. The $I_{ESR}T-T$ plot can be fitted by the Bleaney−Bowers equation for the two-site Hisenberg Hamiltonian $H = -2JS_1 \cdot S_2$, giving the singlet−triplet energy gap ΔE_{S-T} = 4.8 kcal mol^{-1}.[30]

dx.doi.org/10.1021/jp5007928 | J. Phys. Chem. A 2014, 118, 1430−1438

$$I_{ESR}T = C_1\frac{3\exp\left(-\frac{2J}{RT}\right)}{1+3\exp\left(-\frac{2J}{RT}\right)} + C_2$$

The reason for the NMR signal broadening can be explained by the thermally excited TBR state of **1_NH**. As in the case of the **1_NH**, ^{1}H NMR signal broadening was observed except for protons in the phenyl group at room temperature in acetone-d_6 and $CDCl_3$. Furthermore, the signal line widths decreases with cooling from room temperature to −60 °C. These observations give a definitive evidence for small ΔE_{S-T} of **1_NH**. The total spin density of the TBR state calculated at the UB3LYP/6-31+G(d,p) level of the theory is mainly distributed over the imidazole ring and two *p*-quinonemethide moieties but quite small on the phenyl and *tert*-butyl groups. This result is consistent with the behavior of the signal broadening observed in the variable temperature ^{1}H NMR spectra of **1_NH** in acetone-d_6.

CONCLUSION

In summary, we developed a novel solvatochromic molecule that shows significant color change via proton tautomeric reaction. The yellow-colored **1_OH** exists as a dominant species in nonpolar solvents, whereas the blue-colored **1_NH** is stabilized in polar solvents. We investigated the relationship between the unique solvatochromic behavior and the electronic structures of the tautomers. **1_OH** has a planar quinoidal structure and completely closed-shell electronic structure. On the other hand, **1_NH** consists of a nonplanar and twisted π-electron system due to the steric hindrance between the bulky *tert*-butyl groups, resulting in decreasing the double bond character and increasing the SBR character. Moreover, **1_NH** shows the ESR signal at room temperature, indicating the small energy gap between the singlet ground state and the thermally accessible excited TBR state. On the other hand, the DFT and TDDFT calculations for the CS state of **1_NH** well explain the experimental results obtained by the X-ray crystallographic analysis and the IR and UV−vis absorption spectroscopy. Thus, it can be concluded that the ground state of **1_NH** is regarded as the singlet state with small contribution of the biradical character. This result is consistent with small value of the singlet biradical character $y = 0.22$ calculated by the CASSCF calculation. To our knowledge, this is the first report of switching of the π-bond strength by solvent polarity. This work would provide a strategy to develop the environmental stimuli-responsive materials.

ASSOCIATED CONTENT

Supporting Information

HPLC chromatogram, UV−vis absorption spectra in various solvents, ^{1}H NMR and ^{13}C NMR spectra, ESR spectra, X-ray crystallographic analysis data, details of the DFT calculations (atomic coordinates and optimized structures). Complete citations for refs 14, 18, and 24 and CIF files. This material is available free of charge via the Internet at http://pubs.acs.org.

AUTHOR INFORMATION

Corresponding Author

*E-mail: jiro_abe@chem.aoyama.ac.jp.

Notes

The authors declare no competing financial interest.

ACKNOWLEDGMENTS

This work was partially supported by the Core Research for Evolutional Science and Technology (CREST) program of the Japan Science and Technology Agency (JST), a Grant-in-Aid for Scientific Research (A) (22245025) from the Ministry of Education, Culture, Sports, Science, and Technology (MEXT), Japan.

REFERENCES

(1) Lapworth, A. The Action of Halogens on Compounds Containing the Carbonyl Group. *J. Chem. Soc.* **1904**, *85*, 30−42.
(2) Watson, H. B. Reactions of Halogens with Compounds Containing the Carbonyl Group. *Chem. Rev.* **1930**, *7*, 173−201.
(3) Watson, J. D.; Crick, F. H. C. Genetical Implications of the Structure of Deoxyribonucleic Acid. *Nature* **1953**, *171*, 964−967.
(4) Goodman, M. F. Mutations Caught in the Act. *Nature* **1995**, *378*, 237−238.
(5) Nissen, P.; Hansen, J.; Ban, N.; Moore, P. B.; Steitz, T. A. The Structural Basis of Ribosome Activity in Peptide Bond Synthesis. *Science* **2000**, *289*, 920−930.
(6) Beak, P.; Fry, F. S. The Equilibrium between 2-Hydroxypridine and 2-Pyridone in the Gas Phase. *J. Am. Chem. Soc.* **1973**, *95*, 1700−1702.
(7) Douhal, A.; Kim, S. K.; Zewail, A. H. Femtosecond Molecular Dynamics of Tautomerization in Model Base Pairs. *Nature* **1995**, *378*, 260−263.
(8) *Organic Photochromic and Thermochromic Compounds*; Crano, J. C., Guglielmetti, R. J., Eds.; Plenum Press: New York, 1999; Vols. *1* and *2*.
(9) Fujiwara, T.; Harada, J.; Ogawa, K. Hydrogen-Bonded Cyclic Dimer Formation in Temperature-Induced Reversal of Tautomerism of Salicylideneanilines. *J. Phys. Chem. A* **2009**, *113*, 1822−1826.
(10) Miura, M.; Harada, J.; Ogawa, K. Temperature-Induced Reversal of Proton Tautomerism: Role of Hydrogen Bonding and Aggregation in 7-Hydroxyquinolines. *J. Phys. Chem. A* **2007**, *111*, 9854−9858.
(11) Ogawa, K.; Harada, J.; Fujiwara, T.; Yoshida, S. Thermochromism of Salicylideneanilines in Solution: Aggregation-Controlled Proton Tautomerization. *J. Phys. Chem. A* **2001**, *105*, 3425−3427.
(12) Reichardt, C. Solvatochromic Dyes as Solvent Polarity Indicators. *Chem. Rev.* **1994**, *94*, 2319−2358.
(13) Furuta, H.; Ishizuka, T.; Osuka, A.; Dejima, H.; Nakagawa, H.; Ishikawa, Y. NH Tautomerism of N-Confused Porphyrin. *J. Am. Chem. Soc.* **2001**, *123*, 6207−6208.
(14) Holschbach, M. H.; Sanz, D.; Claramunt, R. M.; Infantes, L.; Motherwell, S.; Raithby, P. R.; Jimeno, M. L.; Herrero, D.; Alkorta, I.; Jagerovic, N.; et al. Structure of a 4-Nitroso-5-aminopyrazole and Its Salts: Tautomerism, Protonation, and E/Z Isomerism. *J. Org. Chem.* **2003**, *68*, 8831−8837.
(15) Chakrasali, R. T.; Rao, C. S.; Ila, H.; Junjappa, H. Cyclocondensation of α-Hydroxyimino-β-alkyl/arylimino-β-methylthioketones with Hydrazine Hydrate: Synthesis of 3(5)-Aryl-5(3)-alkyl/arylamino-4-nitroso (or amino) Pyrazoles. *J. Heterocycl. Chem.* **1993**, *30*, 129−134.
(16) Sheldrick, G. M. *SHELXS-97 and SHELXL-97*; University of Gottingen: Germany, 1997.
(17) Sheldrick, G. M. *SADABS*; University of Gottingen: Germany, 1996.
(18) Frisch, M. J.; Trucks, G. W.; Schlegel, H. B.; Scuseria, G. E.; Robb, M. A.; Cheeseman, J. R.; Scalmani, G.; Barone, V.; Mennucci, B.; Petersson, G. A.; et al. *Gaussian 09*, Revision D.01; Gaussian, Inc.: Wallingford, CT, 2009.
(19) Okazaki, T.; Ogawa, K.; Kitagawa, T.; Takeuchi, K. trans-2,2′-Bi(1-phenyladamantylidene): The Most Twisted Biadamantylidene. *J. Org. Chem.* **2002**, *67*, 5981−5986.
(20) Piotrowiak, P.; Strati, G. Singlet Biradical → Singlet Zwitterion Optical Transition in a Twisted Olefin. *J. Am. Chem. Soc.* **1996**, *118*, 8981−8982.

(21) Salem, L.; Rowland, C. The Electronic Properties of Diradicals. *Angew. Chem., Int. Ed.* **1972**, *11*, 92−111.
(22) Yamada, S.; Nakano, M.; Nagao, H.; Yamaguchi, K. Electron Correlation and Structure Dependencies of the Second Hyperpolarizability of Ethylene. *Int. J. Quantum Chem.* **1999**, *71*, 177−183.
(23) Nakano, M.; Kishi, R.; Nitta, T.; Kubo, T.; Nakasuji, K.; Kamada, K.; Ohta, K.; Champagne, B.; Botek, E.; Yamaguchi, K. Second Hyperpolarizability (γ) of Singlet Diradical System: Dependence of γ on the Diradical Character. *J. Phys. Chem. A* **2005**, *109*, 885−891.
(24) Kang, H.; Facchetti, A.; Jiang, H.; Cariati, E.; Righetto, S.; Ugo, R.; Zuccaccia, C.; Macchioni, A.; Stern, C. L.; Liu, Z.; et al. Ultralarge Hyperpolarizability Twisted π-Electron System Electro-Optic Chromophores: Synthesis, Solid-State and Solution-Phase Structural Characteristics, Electronic Structures, Linear and Nonlinear Optical Properties, and Computational Studies. *J. Am. Chem. Soc.* **2007**, *129*, 3267−3286.
(25) Bruckmann, P.; Salem, L. Coexistence of Two Oppositely Polarized Zwitterionic Forms on the Lowest Excited Singlet Surface of Terminally Twisted Butadiene. Two-Funnel Photochemistry with Dual Stereochemistry. *J. Am. Chem. Soc.* **1976**, *98*, 5037−5038.
(26) Noodleman, L. Valence Bond Description of Antiferromagnetic Coupling in Transition Metal Dimers. *J. Chem. Phys.* **1981**, *74*, 5737−5743.
(27) Norman, J. G.; Ryan, P. B.; Noodleman, L. Electronic Structure of 2-Fe Ferredoxin Models by X.alpha. Valence Bond Theory. *J. Am. Chem. Soc.* **1980**, *102*, 4279−4282.
(28) Noodleman, L.; Norman, J. G. The X Valence Bond Theory of Weak Electronic Coupling. Application to the Lowlying States of $Mo_2Cl_8^{4-}$. *J. Chem. Phys.* **1979**, *70*, 4903−4906.
(29) Spanget-Larsen, J.; Gil, M.; Gorski, A.; Blake, D. M.; Waluk, J.; Radziszewski, J. G. Vibrations of the Phenoxyl Radical. *J. Am. Chem. Soc.* **2001**, *123*, 11253−11261.
(30) Bleaney, B.; Bowers, K. D. Anomalous Paramagnetism of Copper Acetate. *Proc. R. Soc. London, Ser. A* **1952**, *214*, 451−465.